RSC Advances

ROYAL SOCIETY OF CHEMISTRY

www.rsc.org/advances

The physicochemical study of polyvinylidene fluoride-Cloisite15A® composite membranes for membrane distillation application

N.M. Mokhtar, W.J. Lau*, A.F. Ismail, B.C. Ng

Advanced Membrane Technology Research Centre (AMTEC), Universiti Teknologi Malaysia, 81310 Skudai, Johor, Malaysia.

*Corresponding author: Tel.: +60 75535926

Email address: lwoeijye@utm.my; lau_woeijye@yahoo.com (W. J. Lau)

Abstract

In this work, polyvinylidene fluoride-Cloisite15A® (PVDF-C15A) hollow fiber membranes were prepared, characterized and evaluated. The membranes were applied to treat dyeing solution via direct contact membrane distillation (DCMD) system. The concentration of the C15A incorporated into the PVDF membrane was varied (3, 5 and 10 wt%) and the corresponding effects were investigated in terms of structural properties and performances. The PVDF-C15A membranes were prepared using dry-jet wet spinning method and characterized with respect to their morphology, porosity, wetting pressure, contact angle, surface roughness, mechanical strength and thermal stability. The presence of the C15A particles was confirmed by Fourier-transform infrared (FTIR), X-ray diffraction (XRD) and scanning electron microscopy with an energy dispersive X-ray spectroscopy (SEM-EDX) analysis. Highly porous membranes with large finger-like structure were shown by the SEM images. The characterization results indicated that the incorporation of C15A particles have shown a significant influence on the physicochemical properties of the membranes. The DCMD experiments revealed that the PVDF membrane incorporated with 3 wt.% C15A (PVDF-3% C15A) exhibited the best MD performance in which complete dye rejection was able to achieve with consistent permeate flux. The promising results obtained by the PVDF-3% C15A membrane is mainly attributed by its improved structural properties resulted from good distribution of C15A particles on the membrane matrix. This study shows that the PVDF membranes incorporated with C15A particles has potential to further improve the performances of pristine PVDF membrane in DCMD of dyeing wastewater.

Keywords: physicochemical, polyvinylidene fluoride, Cloisite15A® clay, membrane distillation, dyeing wastewater

Highlights

- Effect of Cloisite15A® on the physicochemical properties of PVDF hollow fiber membrane were studied.
- Membrane wetting pressure, contact angle, pore size, surface roughness, mechanical strength and melting temperature were reported to increase upon clay addition.
- Permeate flux of PVDF-Cloisite15A® membranes is higher than the neat PVDF membrane.

1 Introduction

The past decade has seen significant advancements in the research and development of membrane distillation (MD). Generally, MD has the potential advantage in liquid-liquid separation process owing to its lower operational and maintenance cost, lower operating hydrostatic pressure/operating temperature, and higher non-volatile solute rejection [1,2]. Nowadays, MD is recognized as an excellent membrane process for various applications such as desalination [3–6], wastewater treatment [7–12], food processing [13], etc. Recently, MD appears as a potential candidate for textile wastewater treatment based on previous studies [7,14–16]. Textile wastewater is extremely hazardous since it contains more than 2000 types of unsafe chemicals, including dyes, de-foamers, bleaches, detergents, etc [17]. Fortunately, heat produced from the effluents could be utilized to operate the MD treatment process which in turn reduces total energy requirement.

From literature, it is found that polypropylene (PP) membranes are commonly used in MD application in treating dyeing solution [7,14–16]. This type of polymer provides higher hydrophobicity, thermal and chemical resistance which are crucial when dealing with hot textile wastewater [18]. However, PP membrane has complicated processability which can only be fabricated either by molten extrusion technique followed by stretching or by thermal phase separation process at high temperature [1]. At present, polyvinylidene fluoride (PVDF) has been preferable as an alternative to PP in the MD process. It is because PVDF exhibits not only similar properties as PP, but also able to dissolve in many common solvents for asymmetric membrane fabrication via phase inversion technique. Recently in 2014, Mokhtar et al. [11] have evaluated the potential of using PVDF membranes in recovering water from hot dyeing solution and have proven that the membranes are excellent to reject at least 99.97% dye molecules during DCMD process.

To date, MD researchers are more interested in developing composite membranes by incorporating polymeric membrane with appropriate amount of inorganic fillers [3,19]. Among various polymers and inorganic composites, PVDF membranes incorporated with montmorillonite (MMT) clays have attracted considerable attention because clays are highly compatible with polymer and relatively abundant. MMT is a common aluminosilicate mineral clay which consists of hydrated aluminium silicates with fine grains and large spaces between the layers as shown in Figure 1(a). Wide variety of modified clays are now commercially

available in the market. These include Cloisite 6A, 10A, 15A, 25A and 30B. These organoclays are distinguished by their *d*-spacing or interlayer distance between the stack layers. Among these modified clays, the Cloisite15A® is a widely used nanofiller for composite membrane because this organically modified MMT exhibits the highest hydrophobicity among other commercially available Cloisite clays [20,21].

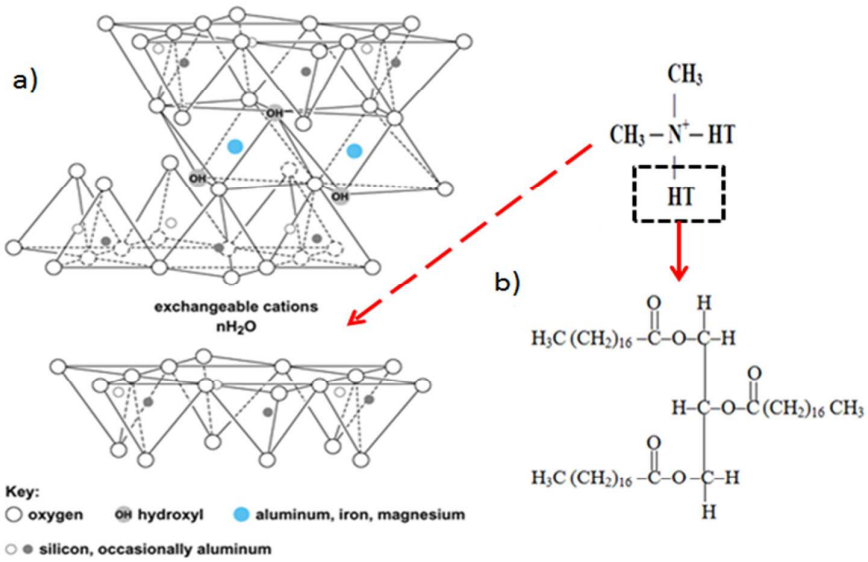

Figure 1 Structure of a) natural MMT and b) dimethyl, dehydrogenated tallow, quaternary ammonium organic modifier [22]

Previous work has shown the importance of clay in improving the properties of PVDF composite which include enhanced melting and crystallization temperatures and membrane toughness [23]. The enhancement in properties can be attributed to the interaction between the cation di-tallow and the PVDF crystalline structure [23–25]. In addition, the improved performances of the PVDF-clay composite membranes have also been reported by MD researchers for desalination process [3,26,27]. Although clay particles have been reported to be useful in improving membrane mechanical stability and melting temperature, a detailed study on the physicochemical properties of the composite membrane and its application on dyeing wastewater treatment has not been reported. Hence, the main objective of this paper is to study the effect of the clay loading on the structural properties of PVDF membrane and how the changes in membrane properties (upon clay incorporation) would alter the membrane performances during DCMD process of dyeing solution.

2 Experimental

2.1 Materials

Polyvinylidene fluoride polymer (PVDF, Kynar® 760) purchased from Arkema Inc., USA was used as a base polymer. Cloisite15A® clay (C15A) was obtained from Southern Clay Products, Inc., USA and was used as received. N-methyl-2-pyrrolidone (NMP, >99.5%) (Merck) was used as a solvent and ethylene glycol (EG, ≥99.5%) (Merck) was used as a non-solvent additive in the polymer solution. Reactive black 5 (RB5, M_w = 991g/mol) from Sigma-Aldrich was used to synthesize dye solution by dissolving it in deionized water produced by ELGA Micromeg Deionizer.

2.2 Fabrication of PVDF hollow fiber membrane

Table 1 Polymer dope composition

Dope / Membrane	PVDF(wt%)	NMP(wt%)	EG(wt%)	[a]C15A(wt%)
PVDF	12	80	8	-
PVDF-3% C15A	12	80	8	3
PVDF-5% C15A	12	80	8	5
PVDF-10% C15A	12	80	8	10

[a]Amount of C15A added into dope solution was determined based on the total weight of PVDF

The PVDF pellets and C15A powder were firstly dried in a vacuum oven overnight at 60±2°C to remove moisture content. A dope solution was prepared by dissolving the PVDF pellets and C15A powder in the NMP and EG mixture, while stirring at 60°C, until the solution became homogeneous. The C15A powder was varied from 3 to 10 wt.% per total weight of PVDF. Another dope solution without clay powder was also prepared to produce a control membrane. The compositions of the dope solutions and their corresponding membrane samples are presented in Table 1. Table 2 shows the spinning conditions applied to all dope formulations. The details of the spinning process can be found elsewhere in our previous work [28]. The as-spun hollow fiber membranes were immersed in water for few days to ensure complete removal of the solvent. The membranes were then post-treated with methanol followed by *n*-hexane to minimize fiber shrinkage during drying at room temperature.

Table 2 PVDF hollow fiber spinning conditions

Spinning conditions	Value
Bore fluid flow rate (mL/min)	2.0
Dope extrusion rate (mL/min)	4.0
Bore fluid composition (wt%)	NMP/H_2O (80:20)
Coagulation medium	Water
Spinneret OD/ID (mm/mm)	1.15/0.55
Air gap distance (mm)	20
Spinning dope temperature (^oC)	25
External coagulation temperature (^oC)	25

2.3 Membrane characterizations

2.3.1 XRD

X-ray diffraction (XRD) analysis was carried out using XRD-X'Pert PRO diffractometer (PANalytical, The Netherlands) using copper Kα (λ = 0.1542 nm at 35 kV and 35 mA) as the source of radiation. The diffractogram was scanned with a scanning rate of 2˚/min in a 2θ range of 1.5–10˚ at room temperature. The *d*-spacing of the C15A in composite was calculated using Bragg's equation based on XRD results:

$$d = \frac{n\lambda}{2\sin\theta} \quad (1)$$

where d is the spacing between layers in the clay structure, λ is the wave length of X-ray equal to 0.154056 nm, θ is the angle at the maximum point of the first peak (lowest θ) in the spectra and n is an integer, representing the order of diffraction where n = 1 in our calculation.

2.3.2 FTIR

Fourier-transform infrared (FTIR) spectra of both C15A powder and membranes were obtained using attenuated total reflectance Fourier transform infrared spectroscope (ATR-FTIR) (Nicolet 5700, Thermo Electron Scientific Instruments Corporation, USA). The spectra were recorded at resolution between 650 and 4000 cm^{-1}.

2.3.3 SEM-EDX

The dry membrane samples were immersed in liquid nitrogen and fractured, followed by sputter-coating with platinum using a sputtering device. The membrane cross-sections of the samples were examined using scanning electron microscope (SEM) (TM-3000, Hitachi). An energy dispersive X-ray (EDX) spectrometer using an acceleration voltage of 15 kV and magnification of 5000× was used for elemental analysis in order to confirm the appearance of C15A particles.

2.3.4 TGA and DSC

Thermal gravimetric analysis of the membrane samples were recorded by thermogravimetry analyzer (Mettler Toledo TGA/SDTA851). The samples were heated from 30 to 800 ^{o}C at a heating rate of 10 ^{o}C/min, under nitrogen atmosphere, with a nitrogen flow rate of 20 mL/min. The melting temperature (T_m) of the hollow fiber membranes was measured using differential scanning calorimetry (Mettler Toledo DSC 822e). The membrane sample was cut into small pieces, weighed and placed into a pre-weighed aluminium crucible. The membrane sample was then heated at temperature ranges of 30–200 ^{o}C at a heating rate of 10 ^{o}C/min in the first cycle to remove the thermal history. The sample was then cooled from 200 to 30 ^{o}C at a cooling rate of 10 ^{o}C/min. The same procedure was repeated in the next heating cycle. T_m of the sample was determined as the midpoint temperature of the transition region in the second heating cycle.

2.3.5 Tensile test

To study the mechanical strength of the fibers, tensile test was performed according to ASTM D3039 standard using an LRX 2.5 SKN Llyod Instrument. The fiber sample was clamped at both ends and pulled in tension at a constant elongation rate of 50 mm/min with an initial gauge length of 50 mm. At least five measurements of the tensile strength, elongation at break and Young's modulus were recorded to yield average result.

2.3.6 AFM

The membranes surface roughness were investigated by atomic force microscope (AFM) (Multimode Nanoscope, DI company). Each membrane sample was cut into small pieces and placed on a square paper card with the size of 1 cm^2 using double-sided adhesive tape. Each surface was scanned in the size of 3μm × 3μm. The surface roughness was expressed in mean surface roughness (R_a).

2.3.7 Liquid entry pressure (LEP) and contact angle measurements

A test module filled with DI water was used before the measurement. One side of the module was attached to a unit of dry hollow fiber membrane while the other was connected to a diaphragm pump. The water was then pressurized slowly into the lumen side of the membrane until its breakthrough pressure. The LEP of membrane was averaged of three repeated measurements. A contact angle goniometer (OCA15plus, DataPhysics), equipped with image-processing software was used to evaluate the degree of membrane hydrophobicity via sessile drop technique. Fifteen spots were measured on each sample and averaged.

2.3.8 Porosity and membrane pore size measurements

The membrane overall porosity (%), ε, which is defined as the volume of the pores per the total volume of the porous membrane was calculated using the following equation [29].

$$\varepsilon\,(\%) = \frac{\dfrac{\left(w_{wet} - w_{dry}\right)}{\rho_w}}{\dfrac{\left(w_{wet} - w_{dry}\right)}{\rho_w} + \dfrac{w_{dry}}{\rho_p}} \times 100 \qquad (2)$$

where ε is the membrane porosity (%), w_{wet} is the weight of wet membrane (g), w_{dry} is the weight of dry membrane (g), ρ_p is the density of the polymer (g/cm^3) and ρ_w is the density of water (g/cm^3).

A PMI capillary flow porometer (Porous Materials Inc., USA) was employed to measure the membrane bubble point and pore size distribution. A bundle of the hollow fibers fully wetted with isopropanol (surface tension = 21.7 dynes/cm) was mounted inside a sample chamber and sealed. Then, pure nitrogen was supplied into the chamber gradually until the pressure reached a point that overcame the capillary flow of the fluid within the largest pore. This point represents the membrane bubble point. The pore size diameter can then be calculated by the following equation.

$$d_p = \frac{4\gamma \cos \phi}{P} \quad (3)$$

where d_p is the pore size diameter, γ is the surface tension of liquid, ø is the contact angle of liquid and P is the external pressure.

2.4 Performance of PVDF hollow fiber membrane in DCMD

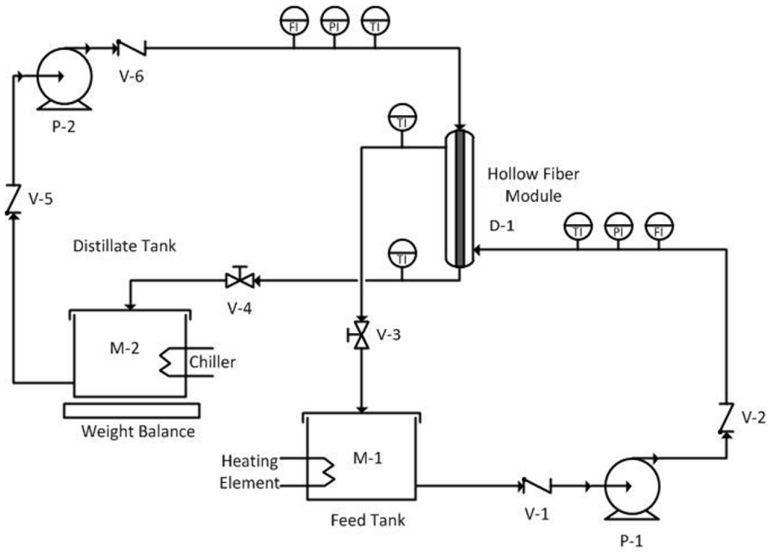

Figure 2 Schematic DCMD experimental setup

A stainless steel module was used to determine the MD performances. The detailed specifications of the module and membranes are listed in Table 3. The DCMD experiments were conducted using a laboratory-scale circulating unit, as illustrated in Figure 2. The DCMD system was designed to have two circulating water streams in which the hot feed stream was circulated through the shell-side while the cold stream through the lumen-side of

the membranes. The hot and cold streams were in counter-current flows to increase energy efficiency. The experiments were carried out under different feed temperatures (50-90ºC) while the inlet temperature of the cold stream was kept constant at 20ºC. Both streams temperatures were controlled by coiled heater (830, PROTECH) and chiller (F26-ED, JULABO), respectively.

Table 3 The details of membrane and membrane module

Membrane	PVDF	PVDF-3%C15A	PVDF-5%C15A	PVDF-10%C15A
Dope composition PVDF/NMP/EG/C15A (g)	(12/80/8/0)	(12/80/8/0.36)	(12/80/8/0.60)	(12/80/8/1.20)
Dope viscosity (cP)	1585	1778	1828	1943
Fiber outer diameter (μm)	813 ± 3	763 ± 19	785 ± 30	789 ± 10
Fiber inner diameter (μm)	527 ± 17	511 ± 15	516 ± 3	516 ± 3
Membrane thickness (μm)	144 ± 38	127 ± 7	132 ± 41	132 ± 41
Module length (mm)	220			
Module inner diameter (mm)	10			
Effective fiber length (mm)	190			
Number of fibers	20			
Effective membrane area (m^2)	~0.0109			

Permeate flux, J of the tested membranes ($kg/m^2.h$) was determined using Equation (4).

$$J = \frac{\Delta W}{A\Delta t} \quad (4)$$

where ΔW (kg) is the weight of permeate collected over a predetermined time Δt (h) and A (m^2) is the effective membrane area. Meanwhile, to determine dye rejection, R (%) of the membranes, Equation (5) was employed.

$$R\,(\%) = \left(1 - \frac{C_p}{C_f}\right) \times 100 \qquad (5)$$

where C_p and C_f are the RB5 concentration (g/L) in the bulk permeate and feed solution, respectively. The concentration of the RB5 was measured by a UV-vis spectrophotometer (DR5000, Hach) with absorbance measured at 597 nm which the maximum absorption occurs.

3. Results and discussion

3.1 XRD analysis

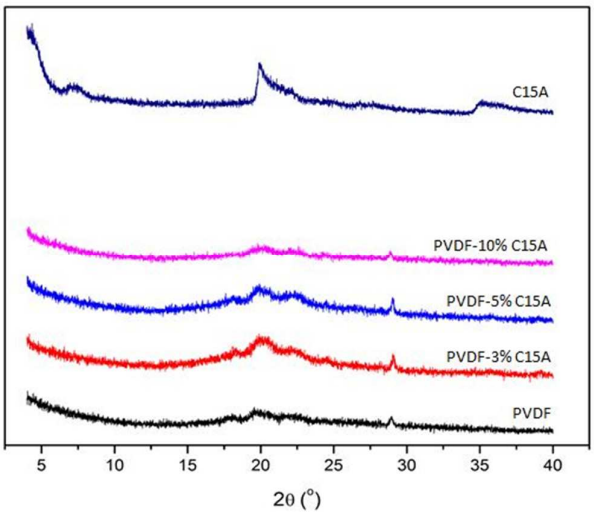

Figure 3 XRD diffractograms for the PVDF-C15A hollow fiber membranes at room temperature

The XRD diffractograms of the C15A and PVDF-C15A membranes of various clay loadings are presented in Figure 3. The C15A powder exhibited two well-defined peaks at 2θ = 7.3˚ and 19.8˚ [30,31]. The corresponding reflection at planes (001) for pure MMT was located at the first peak which is equivalent to basal spacing, d_{001} of 1.21 nm (calculated according to the Bragg equation). However, no obvious peak representing the C15A was found in the XRD diffractograms for all the PVDF-C15A membranes which might indicate that the C15A minerals were exfoliated and well-dispersed in the PVDF matrix. Villaluenga et al. [30] stated that the exfoliation is achieved when the diffraction peak (d_{001}) is no longer observed in the XRD result. This implies that the clay layers have been completely separated

and the individual layers are distributed throughout the polymer matrix. However, conclusions based solely on XRD patterns are only tentative when concerning the mechanism of composite formation and their structure. To supplement the deficiencies of XRD, a specific characterization using transmission electron microscope (TEM) is needed to confirm the clay dispersion in the membrane matrix. However, such analysis is not able to perform in this study due to our limitations to access to this equipment.

Characteristic 2θ peaks for the control PVDF membrane at 17.9˚, 19.7˚, 28.9˚ are corresponded to α (100), α (110) and α (111) with *d*-spacing of 0.495, 0.450, 0.309 nm, respectively [23]. The presence of these peaks also indicates that the PVDF membrane is in α-form crystals. In the case of PVDF-C15A membranes, there was no significant difference between the XRD diffractograms of the PVDF and PVDF composite membranes except for PVDF-10% C15A, which showed the peak intensities of α (100), α (110) and α (111) were slightly reduced. The reduced intensities of α-form diffraction peaks suggested the presence of disordered layer structure due to the intercalation of the polymer in the silicate layers.

3.2 FTIR analysis

Figure 4 compares the ATR-FTIR spectra of the PVDF-C15A membranes with control PVDF membrane and C15A powder. Results from Figure 4(a) is important to determine any changes in the chemical bonds and molecular structure of the composite membranes. Similar peaks at 763, 876, 1072 and 1180 cm^{-1} were observed for all PVDF-C15A membranes (regardless of C15A loadings) which represent the *α*-phase of the PVDF membrane [23,32,33]. Another several peaks were observed at 840, 1276 and 1400 cm^{-1} which could be attributed to *β*-phase [34]. Meanwhile, for Figure 4(b), one can observe that all the PVDF-C15A spectra displayed weak absorption bands of MMT at ~2850 and ~2920 cm^{-1} which are corresponded to the symmetric and asymmetric stretching vibrations of the methylene group ($–CH_2–$) of the guest molecules [35]. Another weak band detected at ~1740 cm^{-1} in the PVDF-C15A membranes could be attributed to the presence of the ester group in the dihydrogenated tallow [36]. The weak band is the typical characteristic of the stretching vibration of the carbonyl (=C=O) group in MMT.

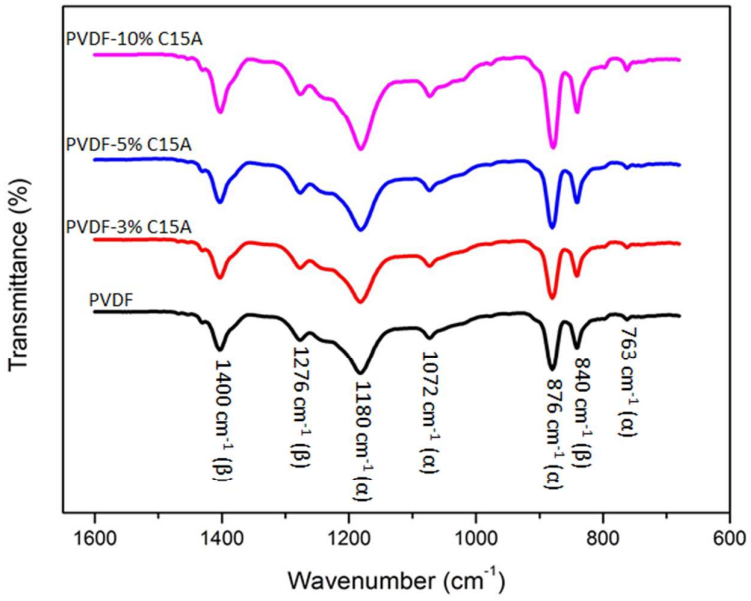

(a)

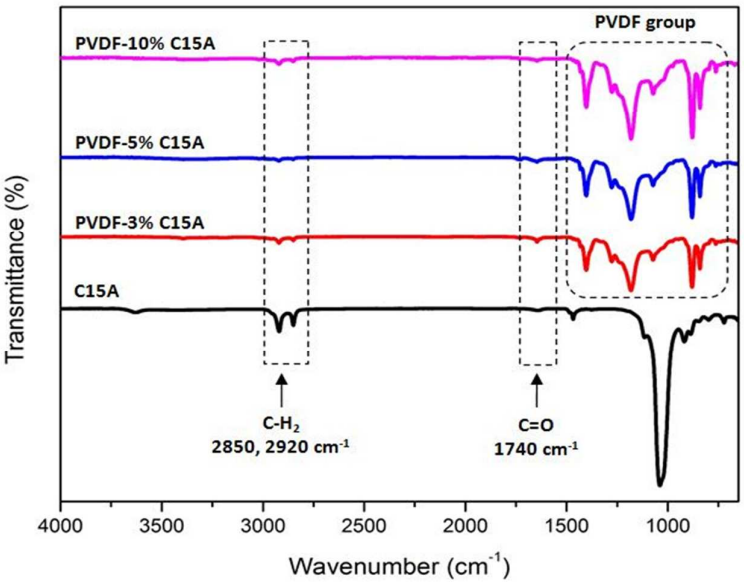

(b)

Figure 4 FTIR-ATR analysis of the PVDF-C15A membranes with a) control PVDF membrane and b) C15A powder

3.3 Morphological analysis

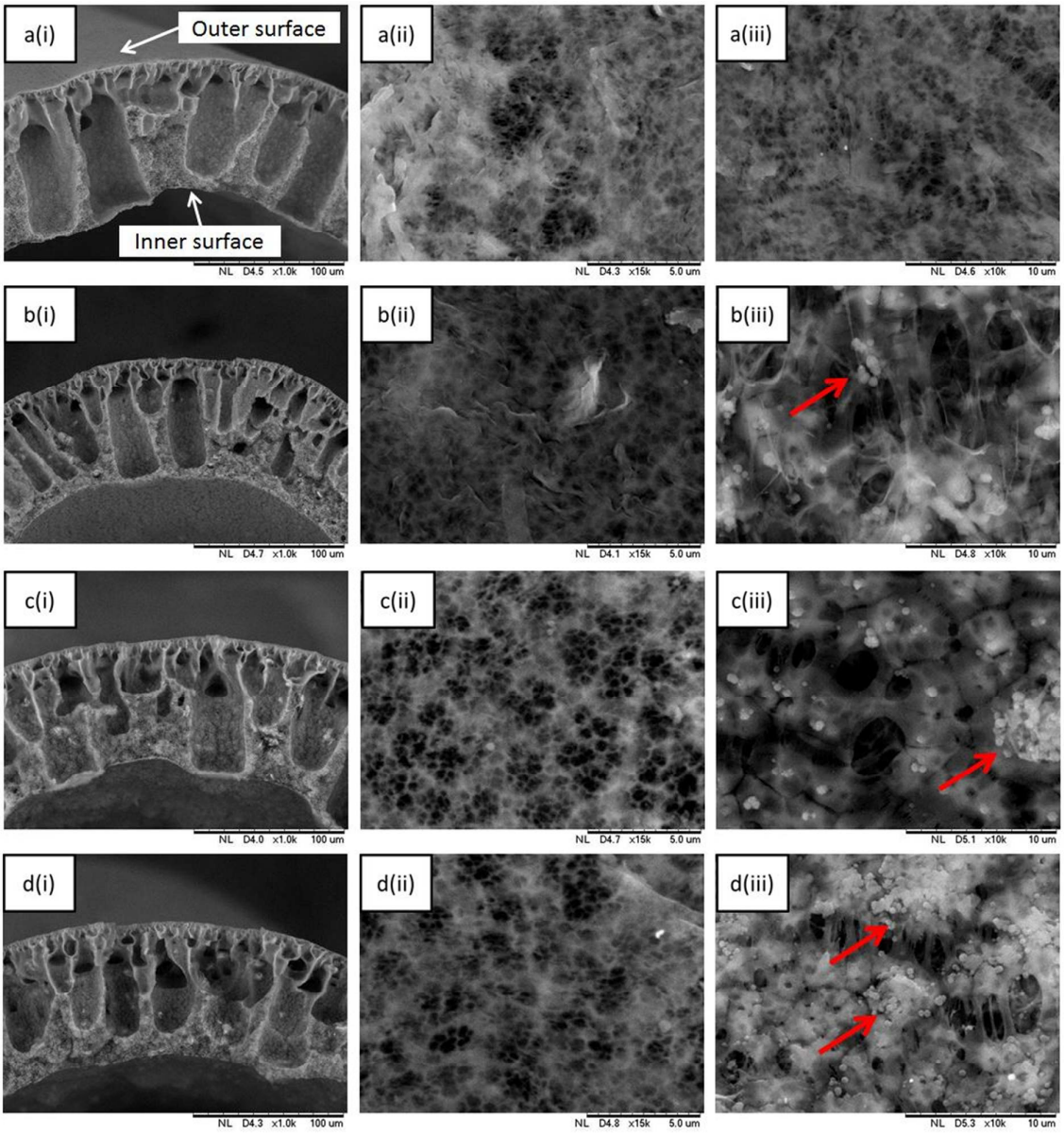

Figure 5 SEM micrographs of PVDF-C15A membranes, (a) PVDF, (b) PVDF-3% C15A, (c) PVDF-5% C15A and (d) PVDF-10% C15A; (i) partial cross-section, (ii) outer surface and (iii) inner surface

The effect of C15A loadings on the structure of the PVDF membranes in macro-scale is presented in Figure 5. As shown in the cross-sectional images, the membrane structure consisted of large finger-like macrovoids stretched from the outer to the inner fiber skin, irrespective of the C15A loadings. It is well-known that narrow finger-like structure is

desirable to reduce the mass resistance during vapor transport [1,11]. Therefore, higher permeate flux is anticipated with the decreasing distance between the finger-like structure and the grounded plate on the membrane cross-sectional morphology. Furthermore, traces of intrusion of nonsolvent coagulant (i.e. water) can be clearly observed. This phenomenon can be explained on the basis of rapid liquid-liquid demixing process which takes place at the outer surface of the fibers due to the following factors: (1) low air gap applied during spinning process, (2) low polymer concentration in the dope solution and (3) high miscibility and compatibility between EG, NMP and water.

Generally, low air gap (20 mm) results in the nascent hollow fiber membrane to have relatively shorter time to solidify before immersing in non-solvent coagulation bath. Such rapid immersion causes great amount of non-solvent and solvent being trapped in the contracted polymer chains. As a result, the polymeric chain interaction becomes less oriented, random and longer-range that eventually produces membranes with larger intermolecular voids and free volume [1,37]. The low polymer concentration used in this study (12 wt% PVDF) tends to produce polymer dope of low viscosity, which also partly contributes to the rapid solvent-non-solvent exchange and solidification during coagulation. It must be pointed out that the dope viscosity was not significantly affected by the clay loadings (see Table 3) as the amount of clay added was considered little based on the weight of dope solution prepared.

In a phase inversion process, the interaction of solvent and non-solvent plays a vital role in determining the membrane morphology which is literally dependent on the thermodynamic and kinetic effects. NMP was used as solvent in this study due to its strong solubility for PVDF and high boiling point. Sukitpaneenit and Chung [38] claimed that PVDF/NMP/water system is the best conditions to have rapid phase separation. In order to improve the membrane porosity, a hydrophilic additive (EG) was employed owing to its ability to enhance the phase inversion rate. As EG has closed solubility parameter with PVDF and water, it can be easily leach out from the membrane matrix during spinning process, leading to the development of porous membrane structure as observed in the SEM images [26].

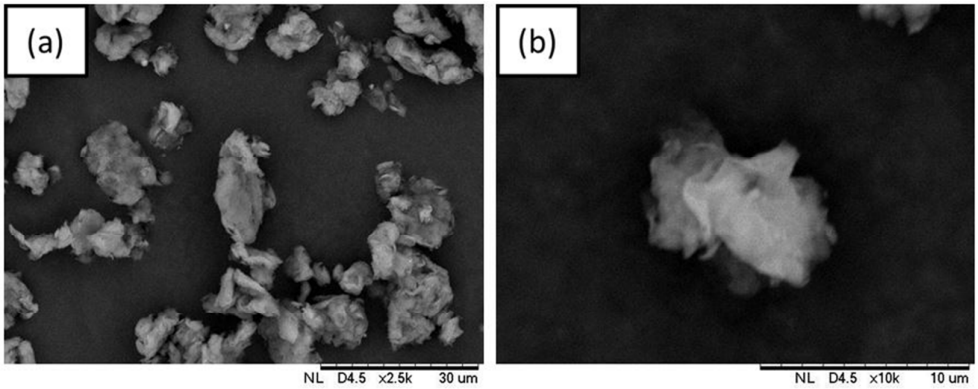

Figure 6 SEM micrographs of C15A particles at different magnifications, (a) 2,500× and (b) 10,000×

The C15A particles were clearly observed on the inner surface of the composite membranes. For PVDF-3% C15A membrane, it can be seen that the C15A particles could disperse quite well on the membrane inner surface without significant agglomeration as indicated by arrow in Figure 5(b)(iii). However, the C15A agglomerates tended to become larger and distributed unevenly on the membrane inner surface when the loading was further increased from 3 wt% to 5 and 10 wt.% as shown in Figure 5(c)(iii) and (d)(iii), respectively. From this observation, it can be concluded that the presence of excessive clay loadings in the membrane matrix could result in larger particle agglomeration. Nevertheless, the micro-agglomerates were still considered relatively smaller (average size = 5.2 ± 0.6 μm) in comparison to the original C15A particle size (average size = 12.5 ± 4.2 μm) as shown in Figure 6. The reported original particle size is in agreement with the information provided by Southern Clay Products, Inc. (US) where 90% of the original dry C15A particle sizes is less than 13 μm while only 10% of that is below 2 μm. Although it is still uncertain whether the composite membranes were fully exfoliated as indicated by the previous XRD results, the SEM images proved that C15A particle sizes were reduced after the blending process and were randomly dispersed on the inner layer of the composite membranes.

According to the EDX results of the membrane inner and outer surface as tabulated in Table 4, it can be said that the detection of silicon (Si), aluminium (Al) and oxygen (O) on the PVDF-C15A membrane strongly indicate the existence of C15A in the membrane matrix. Generally, one can see the increase of these elements in particular Si with increasing C15A loadings in the membrane. It is also worth to note that increasing Si element in membranes has been previously reported to enhance the membrane porosity and hydrophobicity which

452 are important criteria for effective MD [39,40]. With respect to membrane overall thickness,
453 it is found that the PVDF-3% C15A possessed the lowest value (see Table 3) which might
454 give it advantage of minimizing mass resistance during MD process.
455
456 **Table 4** EDX quantitative analysis of PVDF and PVDF-C15A composite membranes

Surface elements (wt%)	PVDF		PVDF-3% C15A		PVDF-5% C15A		PVDF-10% C15A	
	inner	outer	inner	outer	inner	outer	inner	outer
F	58.44	56.84	56.18	54.47	55.55	55.10	53.80	51.69
C	41.56	43.16	39.80	40.68	40.19	40.75	40.52	41.43
O	-	-	3.62	4.30	3.40	3.48	4.16	4.79
Si	-	-	0.26	0.38	0.59	0.51	1.06	1.53
Al	-	-	0.14	0.17	0.27	0.16	0.46	0.56
Total elements	100	100	100	100	100	100	100	100

457
458 **3.4 Thermal stability study**
459
460 As shown in Figure 7, the thermogravimetric (TG) curves of C15A powder decreased
461 when the decomposition temperature increased from 200 to 460˚C due to the decomposition
462 of intercalated organic groups trapped inside the MMT gallery. Based on the derivative
463 thermogravimetric (DTG) curve, the major weight loss occurred at 304˚C could be related to
464 the loss of the organic groups in the clay sample [36]. Oades and Townsend [41] reported that
465 90% of the total carbon from the clay sample will be oxidized at temperature above 430˚C.
466 Meanwhile, for TG curve of the PVDF sample, the membrane decomposed rapidly after
467 300˚C. It has been widely reported that the thermal decomposition of the PVDF polymer
468 begins to generate hydrogen fluoride (HF) gas at 315˚C and its evolution becomes rapid at
469 370˚C [42]. The high T_d of the PVDF membrane which is at 474˚C indicates the excellent
470 thermal stability of this kind of polymer. The T_d represents the temperature of the maximum
471 rate of decomposition that can be identified from the DTG curve.
472

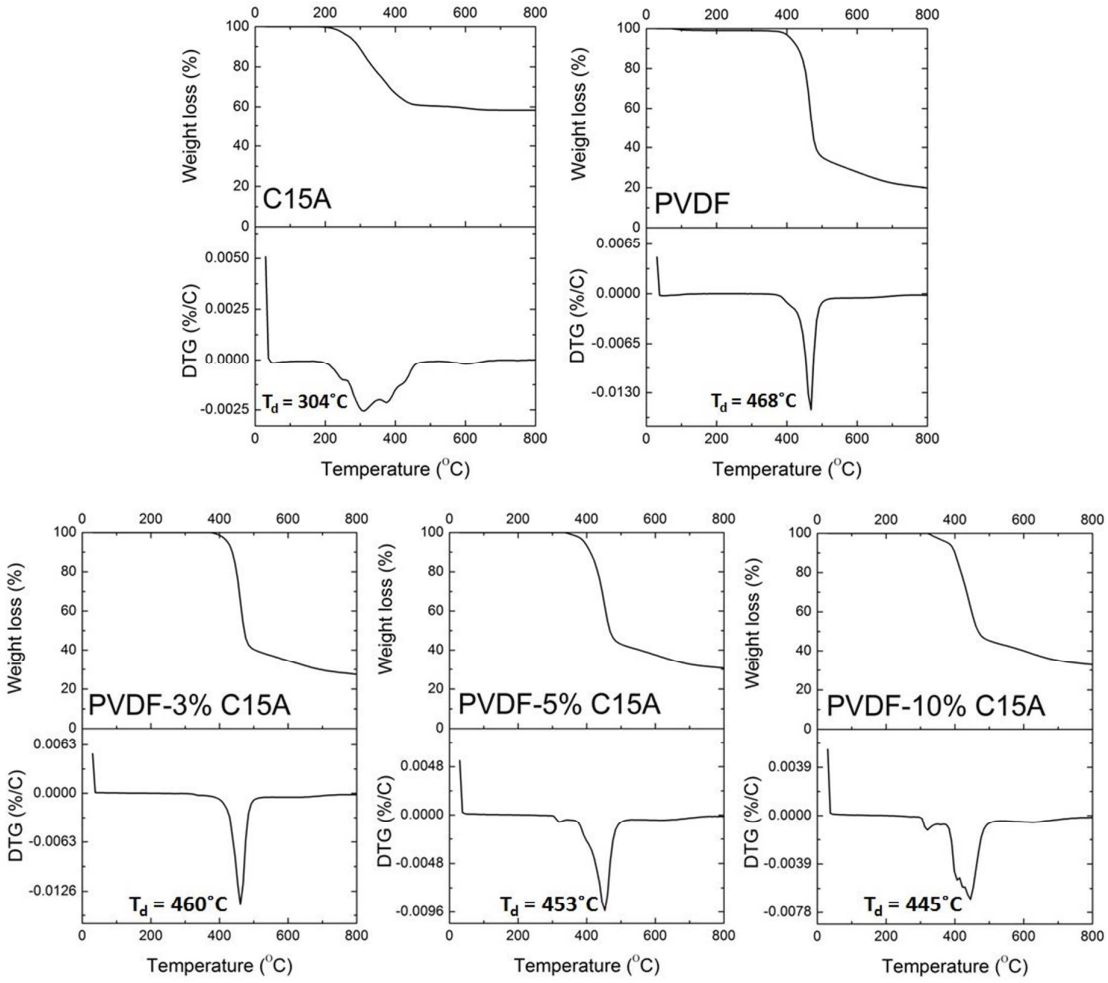

Figure 7 TG and DTG curves for C15A powder, PVDF membrane and PVDF-C15A membranes of various clay loadings

For the PVDF-C15A samples, a major weight loss occurred in the range of 320–470˚C was observed, which is due to the decomposition of PVDF. The C15A addition has caused all the composite membranes to have lower T_d than that of the control PVDF membrane. Generally, composites are expected to exhibit better thermal stability due to the incorporation of inorganic fillers. On the contrary, opposite effect was shown in this work in which the incorporation of the C15A in the PVDF membranes have decreased the thermal stability of the PVDF matrix. This is likely because C15A particles which form weaker bonds with the PVDF polymer chains tend to decompose easily after 304˚C. Besides, it is also suggested that the C15A might react with the byproduct released by the decomposing PVDF, i.e. HF, thus further accelerated the decomposition process [43]. At 800˚C, the weight loss of the composite membranes reduced from 80% to 67% with increasing C15A loadings from

zero to 10 wt%. This revealed the role of the C15A particles in reducing the amount of degradable PVDF matrix. However, the T_d values were increased with the loadings. From the DSC analysis, it is found that the melting temperature (T_m) of composite membranes were increased slightly to 170˚C from 165˚C as shown by the control membrane, suggesting the clay particles might influence the crystallization process of the PVDF-C15A membranes and their flexibility of polymer chains.

3.5 Mechanical stability study

Table 5 Mechanical properties of PVDF and PVDF-C15A composite membranes

Membrane	Tensile stress (MPa)	Elongation at break (%)	Young's modulus (GPa)
PVDF	7.48 ± 0.72	161.53 ± 8.91	25.01 ± 0.70
PVDF-3% C15A	8.54 ± 0.58	148.63 ± 2.22	29.55 ± 2.92
PVDF-5% C15A	8.51 ± 0.81	72.13 ± 4.38	24.72 ± 1.41
PVDF-10% C15A	6.89 ± 0.50	41.19 ± 1.38	19.24 ± 2.23

Table 5 presents the mechanical properties of the membrane samples. The tensile strength increased slightly upon clay addition except in the sample having 10 wt% C15A. On the contrary, the elongation at break decreased dramatically with increasing clay concentrations. With respect to Young's modulus, a significant enhancement was observed with PVDF membrane incorporated with 3 wt% C15A. As expected, the clay particles affected the crystallization process of the PVDF-C15A membrane and improved the tensile strength as well as Young's modulus. However, excessive loading of clay particles might lead to significant agglomeration which consequently results in weak points for the membranes. When the loading is increased to 10 wt%, the massive amounts of C15A particles tend to restrict the space for free movement of PVDF chain, decreasing the mechanical strength. In addition, the negative impact on the elongation at break suggested the presence of disrupted molecular structure due to large aspect ratio and interaction between clay particles and the membrane matrix, which can be a result of hindered slippage of polymer chains between MMT layers [44,45]. These results are in good agreement with the XRD and DSC results reported earlier.

3.6 AFM results and membrane characteristics

Figure 8 shows the 3D AFM images of the PVDF and PVDF-C15A composite membranes together with surface roughness value. The AFM images clearly showed that the PVDF membrane had a relatively smoother surface than the PVDF-C15A membranes. The surface roughness of the outer layer of the PVDF-C15A membranes increased with the clay loading which is likely due to the higher clay agglomeration.

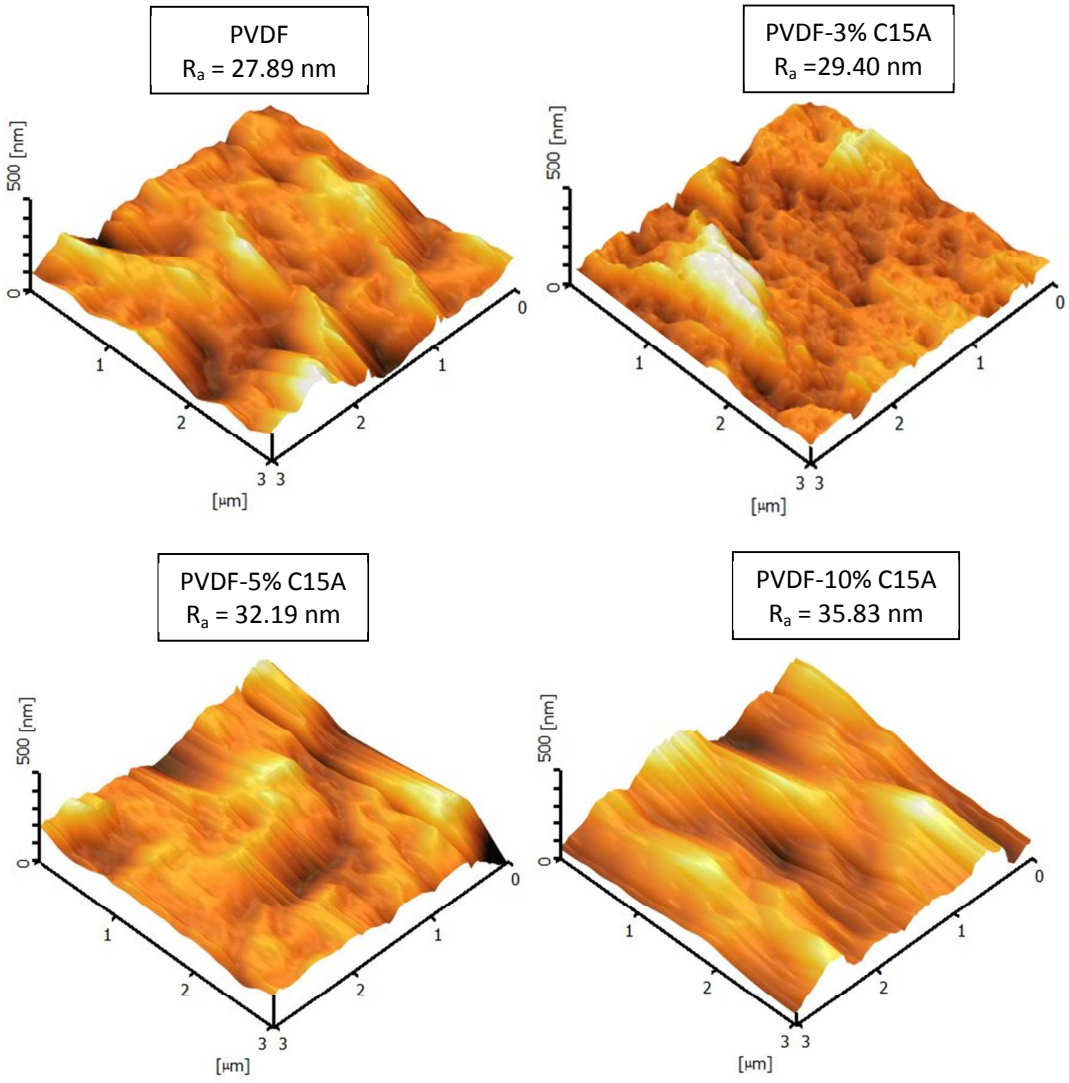

Figure 8 3D AFM images of the outer surfaces of the PVDF and PVDF-C15A membranes together with R_a value

536 **Table 6** Characteristics of the PVDF and PVDF-C15A membranes

Membrane	LEP (psi)	CA (˚)	ε (%)	d_p (μm)
PVDF	2.90	88.85 ± 2.85	82.74 ± 0.66	0.0444
PVDF-3% C15A	13.05	97.72 ± 2.54	83.70 ± 0.67	0.0880
PVDF-5% C15A	7.25	91.43 ± 1.09	83.02 ± 0.73	0.1082
PVDF-10% C15A	5.80	93.07 ± 0.75	83.03 ± 0.83	0.1443

537

538 Table 6 summarizes several properties of the membranes which are important for MD
539 process. It can be seen that the incorporation of C15A particles significantly improved the
540 membrane characteristics in terms of wetting pressure, hydrophobicity and mean pore size.
541 This might indicate that the arrangement of polymer chain packing has been disordered by
542 the presence of clay particles in the membrane matrix, leading to better structural properties.
543 The higher LEP value obtained by the composite membranes showed that the membranes are
544 able to prevent liquid penetration through the membrane pores due to the cross-membrane
545 pressure difference that is sometimes caused by imbalance of feed and permeate side
546 pressures.

547

548 Furthermore, the addition of C15A also increased the contact angle of the PVDF-
549 C15A membranes, which is mainly due to the higher surface roughness. This phenomenon
550 can be explained by the famous theory of Wenzel or Cassie effect, as the presence of air
551 pockets underneath the rough surface tends to hinder the liquid from penetrating into the
552 grooves, which in turn increases surface hydrophobicity [46,47]. From the data obtained, no
553 precise trend can be established between the contact angle value and the clay concentration.
554 This result might be attributed to other factors such as size of the surface heterogeneities and
555 asperities as well as surface cleanliness during contact angle measurements [48].

556

557 In addition, a significant improvement with respect to mean pore size was recorded.
558 Generally, the mean pore size is used to determine vapour flux, and bigger mean pore size
559 (within MD range of 0.01–1.0 μm) is required for higher permeate flux. The improvement on
560 the membrane porosity with respect to the C15A incorporation was insignificant in this study
561 as all the membranes displayed reasonably high porosity (>82%). It is thus believed that the
562 high porosity of the fabricated membranes is mainly due to the low concentration of polymer
563 used and the EG contribution.

3.7 Effect of clay loadings on DCMD experiments

3.7.1 DCMD tested using DI water

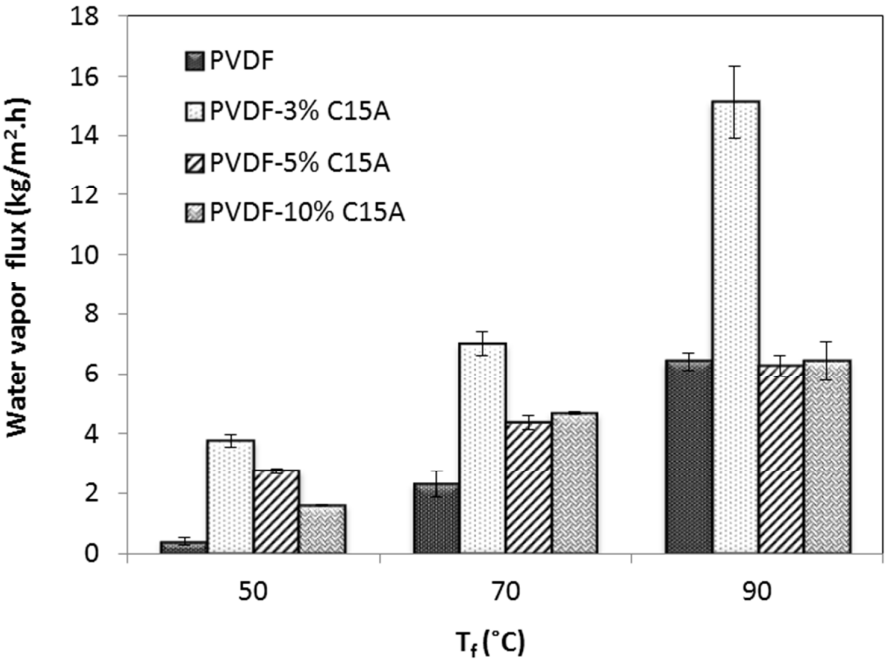

Figure 9 Effect of different clay loadings on the water vapor flux of PVDF-C15A hollow fiber membranes (Conditions = hot stream: flow rate of 0.023 m/s, cold stream: 20˚C at flow rate of 0.010 m/s)

In this study, a DCMD test was carried out using DI water as the feed and distillate solutions. The objective of this experiment is to study the effect of different clay loadings on the DCMD performances in terms of water vapor flux at different feed temperatures. Feed temperature is a crucial operating parameter in MD process since the MD is driven by temperature gradient which promotes partial pressure of volatile compounds to initiate permeation. Water is the main permeate species for MD process because it is volatile at any temperature. Figure 9 shows the effect of feed temperature (T_f) on the permeate flux of PVDF membranes in the range of 50–90˚C.

As shown in Figure 9, PVDF-C15A composite membranes exhibited better performance compared to the neat PVDF membrane at feed temperatures of 50 and 70˚C. In this study, the presence of clay particles in the membrane has significant effect on the permeate flux which can be correlated to membrane structural and physical characteristics e.g. mean pore size, hydrophobicity, wetting pressure as discussed in the previous section. It

is well-known that larger mean pore size is desirable for MD membrane to decrease the mass transport resistance and enhance the permeate flux [1]. Meanwhile, the increase of membrane hydrophobicity and wetting pressure with the incorporation of clay particles could avoid water penetration from both sides and minimize the membrane wetting problem [3].

With respect to different clay loadings, the membrane incorporated with 3% C15A showed the excellent performance at every T_f among the studied membranes. Although the structures of the PVDF and PVDF-C15A composite membranes are very similar, the remarkable improvement of permeate flux of PVDF-3% C15A membrane can be correlated to the lower vapor transport resistance in the membrane module. Since PVDF-3% C15A has the lowest membrane thickness, lower mass resistance during vapor transport can be expected [49]. Because of this reason, the pure water vapor flux achieved by the membrane was close to 2.4 times higher than the PVDF and other composite membranes at $T_f = 90^{\circ}C$. Meanwhile, the higher wetting pressure and hydrophobicity of the prepared membrane in comparison with the other composite membranes had also made the PVDF-3% C15A to achieve the highest water vapor flux. Furthermore, this membrane has an optimum mean pore size and higher mechanical strength that could potentially retain liquid water from passing through membrane pores easily.

From Figure 9, it is noticed that the permeate flux for each membrane was increased with feed temperature. In MD application, it is well-accepted that higher feed temperatures would result in greater flux since it generates more water vapor to diffuse through the pores of the membrane surface followed by condensation on the permeate side. Susanto [50] reported that higher feed temperatures would increase the permeate flux exponentially at the expense of slight deterioration in selectivity since more compounds in the feed solution would vaporize. However, it must be noted that polarization due to temperature and concentration might also cause the permeate flux to fluctuate.

3.7.2 DCMD tested using dyeing solution

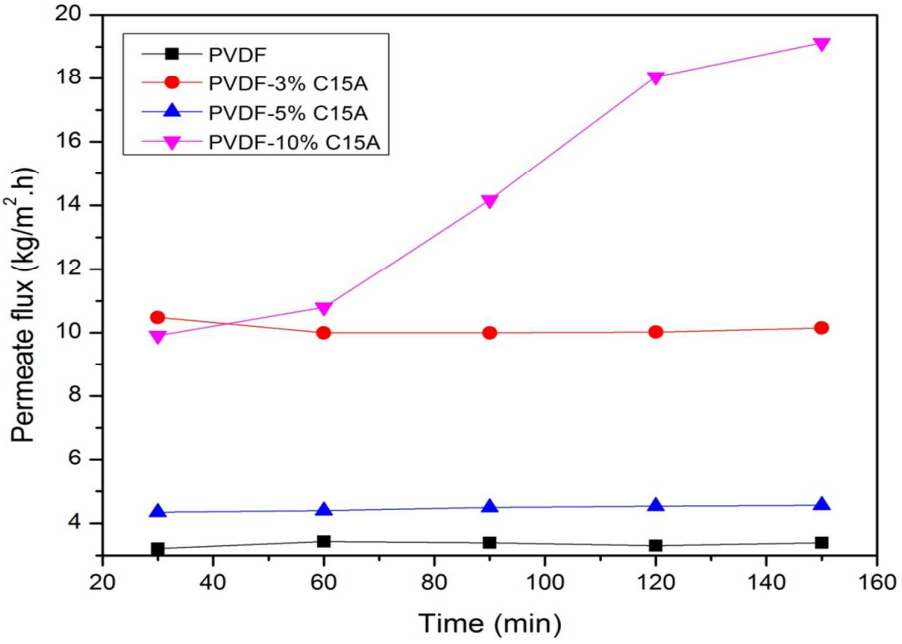

(a)

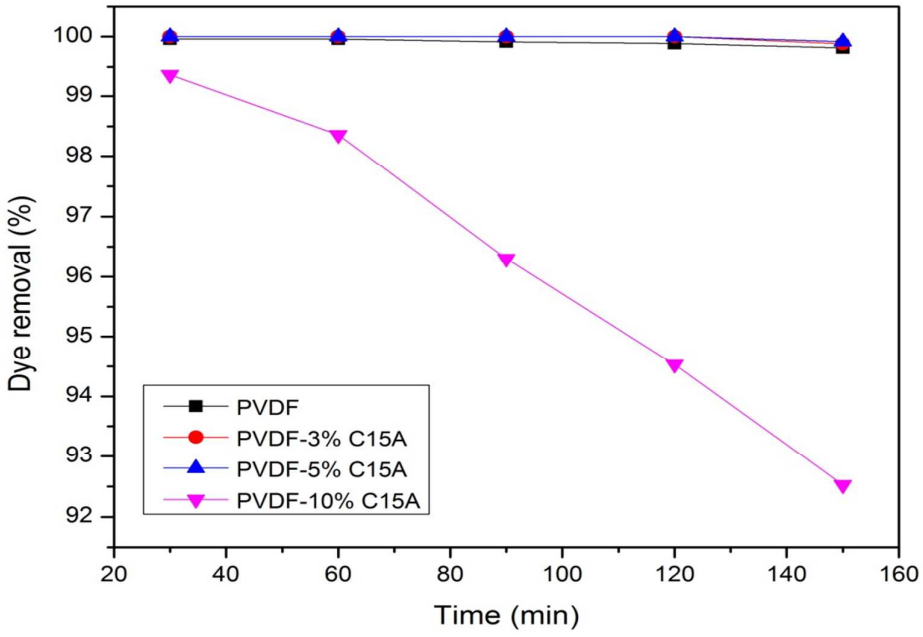

(b)

Figure 10 Permeate flux (a) and dye removal (b) of PVDF-C15A hollow fiber membranes as a function of feed temperature (Conditions = hot stream: 70˚C at flow rate of 0.023 m/s, cold stream: 20˚C at flow rate of 0.010 m/s)

The performance of the composite membranes was further evaluated in the DCMD process to treat dyeing solution. Figure 10 shows the permeate fluxes and dye removal of PVDF and PVDF-C15A membranes as a function of filtration time using feed solution containing 0.05 g/L RB5. In this work, only water vapor can pass through the pores from the feed side while the dye molecule will be retained and recycled back to the feed tank. Generally, the water vapor transport is based on vapour/liquid equilibrium (VLE) principle in which both heat and mass transfer occur simultaneously through the membrane [2].

From that figure, it can be seen that each membrane showed a very consistent flux throughout the MD test except for the PVDF-10% C15A. With respect to dye removal, all membranes demonstrated consistent separation efficiency with average dye rejection of 99.9% except for the PVDF-10% C15A membrane which decreased gradually from 99.3% to 92.5%. As expected, the PVDF membrane incorporated with 3% C15A perfomed the best throughout the study with respect to permeate flux and percentage of dye removal. The permeate flux results are in accordance with the previous experiment in which DI water was used as feed. It can be seen that PVDF-3% C15A produced a consistent flux around 10.1 $kg/m^2.h$ with a complete dye rejection at the permeate side. Almost 70% flux enhancement was recorded in comparison to the control PVDF membrane.

In DCMD, both water flux and solute removal are crucial parameters that one must take into account to determine membrane performance. Basically, the membrane itself acts only as a physical barrier to hold the liquid–vapor interface at the entrance of the membrane pores. However, it is important to note that the structural properties of the membrane also play a vital role to the MD performances. Since PVDF-3% C15A has the highest LEP and contact angle values, this membrane tends to has greater capability to prevent liquid intrusion into the membrane pores [3]. Moreover, the mean pore size of this membrane is the smallest compared to other composite membranes which minimizes its wetting tendency. Meanwhile, the promising flux obtained by this membrane is mainly due to its lower membrane thickness and higher overall porosity which decreases the mass transfer resistance across the membrane [11]. Although PVDF-3% C15A has the lowest membrane thickness, its tensile strength and Young's modulus are higher than the control PVDF and other PVDF-C15A composite membranes. This is mainly due to the good distribution of the clay particles on the membrane matrix which improves the mechanical properties of the membrane [45]. The mechanical stability of the prepared membrane is of particular concern for the long-term study. Based on

the results obtained, it can be concluded that C15A can act as a good filler for the PVDF membrane, enhancing not only the structure properties of the membrane but also significantly improve the permeate flux without sacrificing dye rejection.

Nevertheless, a rapid increment of flux by the PVDF-10% C15A membrane was observed after 1 h of the operation and this might be caused by structural defects on the membranes which allows the feed solution to pass through the pores easily. Therefore, it is believed that the membrane produced from the highest C15A loading is unable to withstand concentrated feed solution due to its insufficient mechanical strength properties as reported in Table 5. Since PVDF-10% C15A contained the highest amount of C15A particles, more defective structures are expected to develop due to the clay agglomeration in the membrane matrix. Such agglomeration would expose the membrane to wetting problem.

4 Conclusion

In this study, the influence of Cloisite15A® clay particles on the physicochemical properties and performances of PVDF membranes has been successfully prepared, characterized and evaluated. The presence of the clay on the membrane surface has been confirmed by the FTIR, XRD and SEM-EDX analysis. The formation of narrow and large finger-like structure in the PVDF membranes is mainly due to several factors; (1) low air gap applied during spinning process, (2) low polymer concentration used in the dope solution and (3) high miscibility and compatibility between EG, NMP and water. Cross-sectional SEM images revealed that the EG addition has dominant effects on the membrane internal, porosity and surface pore structure, regardless of the clay loadings. A significant increment on the structural properties (e.g. LEP, contact angle, surface roughness, tensile strength, Young's modulus, melting temperature) have been observed after the incorporation of small loading of C15A (3 wt.%) into the PVDF membrane. DCMD experiments conducted using DI water as feed indicated that the PVDF-3% C15A had the highest pure water vapor flux (15.1 $kg/m^2.h$) at $T_f = 90^{\circ}C$ compared to 6.4 $kg/m^2.h$ shown by the control PVDF membrane. During DCMD experiments with dyeing solution, the PVDF-3% C15A demonstrated the most promising performance by producing around 10 $kg/m^2.h$ permeate sample free of any dye molecule. In conclusion, the incorporation of Cloisite15A® clay onto the PVDF membranes could improve not only membrane structural properties, but also its performances during MD process.

Acknowledgement

The authors gratefully acknowledge Universiti Teknologi Malaysia (UTM) for funding this project under Research University Grant (Tier 1) (Vot No: Q.J130000.2509.05H48, Title: Separation and Purification of Textile Wastewater using Low-Energy Direct Contact Membrane Distillation (DCMD) Process).

References

[1] M. Khayet, T. Matsuura, Membrane distillation and principles, Elsevier Science, Amsterdarm, 2011.
[2] A. Alkhudhiri, N. Darwish, N. Hilal, Membrane distillation: A comprehensive review, Desalination. 287 (2012) 2–18.
[3] J.A. Prince, G. Singh, D. Rana, T. Matsuura, V. Anbharasi, T.S. Shanmugasundaram, Preparation and characterization of highly hydrophobic poly(vinylidene fluoride) – Clay nanocomposite nanofiber membranes (PVDF–clay NNMs) for desalination using direct contact membrane distillation, J. Membr. Sci. 397–398 (2012) 80–86.
[4] A. Alkhudhiri, N. Darwish, N. Hilal, Treatment of high salinity solutions: Application of air gap membrane distillation, Desalination. 287 (2012) 55–60.
[5] H. Chang, S.G. Lyu, C.M. Tsai, Y.H. Chen, T.W. Cheng, Y.H. Chou, Experimental and simulation study of a solar thermal driven membrane distillation desalination process, Desalination. 286 (2012) 400–411.
[6] K.C. Chong, S.O. Lai, K.M. Lee, W.J. Lau, A.F. Ismail, B.S. Ooi, Characteristic and performance of polyvinylidene fluoride membranes blended with different additives in direct contact membrane distillation, Desal. Wat. Treat. (2014) doi:10.1080/19443994.2014.910139.
[7] A. Criscuoli, J. Zhong, A. Figoli, M.C. Carnevale, R. Huang, E. Drioli, Treatment of dye solutions by vacuum membrane distillation, Water Res. 42 (2008) 5031–7.
[8] A. El-Abbassi, A. Hafidi, M. Khayet, M.C. García-Payo, Integrated direct contact membrane distillation for olive mill wastewater treatment, Desalination. 323 (2013) 31–38.
[9] S. Goh, J. Zhang, Y. Liu, A.G. Fane, Fouling and wetting in membrane distillation (MD) and MD-bioreactor (MDBR) for wastewater reclamation, Desalination. 323 (2013) 39–47.
[10] K. Gethard, O. Sae-Khow, S. Mitra, Carbon nanotube enhanced membrane distillation for simultaneous generation of pure water and concentrating pharmaceutical waste, Sep. Purif. Technol. 90 (2012) 239–245.
[11] N.M. Mokhtar, W.J. Lau, A.F. Ismail, The potential of membrane distillation in recovering water from hot dyeing solution, J. Water Process Eng. 2 (2014), 71–78.
[12] N.M. Mokhtar, W.J. Lau, B.C. Ng, A.F. Ismail, D. Veerasamy, Preparation and characterization of PVDF membranes incorporated with different additives for dyeing solution treatment using membrane distillation, Desal. Wat. Treat. (2014) doi:10.1080/19443994.2014.959063.
[13] A. Hausmann, P. Sanciolo, T. Vasiljevic, M. Weeks, K. Schroën, S. Gray, M. Duke, Fouling of dairy components on hydrophobic polytetrafluoroethylene (PTFE) membranes for membrane distillation, J. Membr. Sci. 442 (2013) 149–159.

[14] F. Banat, S. Al-Asheh, M. Qtaishat, Treatment of waters colored with methylene blue dye by vacuum membrane distillation, Desalination. 174 (2005) 87–96.
[15] S. Mozia, A.W. Morawski, M. Toyoda, T. Tsumura, Integration of photocatalysis and membrane distillation for removal of mono- and poly-azo dyes from water, Desalination. 250 (2010) 666–672.
[16] D. Qu, Z. Qiang, S. Xiao, Q. Liu, Y. Lei, T. Zhou, Degradation of Reactive Black 5 in a submerged photocatalytic membrane distillation reactor with microwave electrodeless lamps as light source, Sep. Purif. Technol. 122 (2014) 54–59.
[17] N. Halimoon, R. Goh, S. Yin, Removal of Heavy Metals from Textile Wastewater using Zeolite, EnvironmentAsia, 3 (2010) 124–130.
[18] M.S. Kang, B. Chun, S.S. Kim, Surface Modification of Polypropylene Membrane by Low-Temperature Plasma Treatment, J. Appl. Polym. Sci. 81 (2001) 1555–1566.
[19] F. Edwie, M.M. Teoh, T.S. Chung, Effects of additives on dual-layer hydrophobic–hydrophilic PVDF hollow fiber membranes for membrane distillation and continuous performance, Chem. Eng. Sci. 68 (2012) 567–578.
[20] P. Daraei, S.S. Madaeni, E. Salehi, N. Ghaemi, H.S. Ghari, M.A. Khadivi, et al., Novel thin film composite membrane fabricated by mixed matrix nanoclay/chitosan on PVDF microfiltration support: Preparation, characterization and performance in dye removal, J. Membr. Sci. 436 (2013) 97–108.
[21] J. Jaafar, A.F. Ismail, T. Matsuura, Preparation and barrier properties of SPEEK/Cloisite 15A®/TAP nanocomposite membrane for DMFC application, J. Membr. Sci. 345 (2009) 119–127.
[22] A.K. Zulhairun, A.F. Ismail, T. Matsuura, M.S. Abdullah, A. Mustafa, Asymmetric mixed matrix membrane incorporating organically modified clay particle for gas separation, Chem. Eng. J. 241 (2014) 495–503.
[23] T.U. Patro, M.V. Mhalgi, D.V. Khakhar, A. Misra, Studies on poly(vinylidene fluoride)–clay nanocomposites: Effect of different clay modifiers, Polymer. 49 (2008) 3486–3499.
[24] W. Yu, Z. Zhao, W. Zheng, Y. Song, B. Li, B. Long, Q. Jiang, Structural characteristics of poly(vinylidene fluoride)/clay nanocomposites, Mater. Lett. 62 (2008) 747–750.
[25] H.Y. Hwang, D.J. Kim, H.J. Kim, Y.T. Hong, S.Y. Nam, Effect of nanoclay on properties of porous PVdF membranes, Trans. Nonferrous Met. Soc. China. 21 (2011) s141–s147.
[26] K.Y. Wang, S.W. Foo, T. Chung, Mixed Matrix PVDF Hollow Fiber Membranes with Nanoscale Pores for Desalination through Direct Contact Membrane Distillation, Ind. Eng. Chem. Res. 48 (2009) 4474–4483.
[27] S. Bonyadi, T.S. Chung, R. Rajagopalan, A novel approach to fabricate macrovoid-free and highly permeable PVDF hollow fiber membranes for membrane distillation, AICHE J. 55 (2009) 828–833.
[28] W.J. Lau, A.F. Ismail, Theoretical studies on the morphological and electrical properties of blended PES/SPEEK nanofiltration membranes using different sulfonation degree of SPEEK, J. Membr. Sci. 334 (2009) 30–42.
[29] S. Chabot, C. Roy, G. Chowdhury, T. Matsuura, Development of poly(vinylidene fluoride) hollow-fiber membranes for the treatment of water/organic vapor mixtures, J. Appl. Polym. Sci. 65 (1997) 1263–1270.
[30] J.P.G. Villaluenga, M. Khayet, M.A. López-Manchado, J.L. Valentin, B. Seoane, J.I. Mengual, Gas transport properties of polypropylene/clay composite membranes, Eur. Polym. J. 43 (2007) 1132–1143.

[31] J. Jaafar, A.F. Ismail, T. Matsuura, Effect of Dispersion State of Cloisite15A® on the Performance of SPEEK/Cloisite15A Nanocomposite Membrane for DMFC Application, J. Appl. Polym. Sci. 124 (2012) 969–977.
[32] G. Mago, D.M. Kalyon, F.T. Fisher, Membranes of Polyvinylidene Fluoride and PVDF Nanocomposites with Carbon Nanotubes via Immersion Precipitation, J. Nanomater. 2008 (2008) 1–8.
[33] Q.Y. Peng, P.H. Cong, X.J. Liu, T.X. Liu, S. Huang, T.S. Li, The preparation of PVDF/clay nanocomposites and the investigation of their tribological properties, Wear. 266 (2009) 713–720.
[34] N.A. Hashim, Y. Liu, K. Li, Stability of PVDF hollow fibre membranes in sodium hydroxide aqueous solution, Chem. Eng. Sci. 66 (2011) 1565–1575.
[35] J.M. Cervantes-Uc, J.V. Cauich-Rodríguez, H. Vázquez-Torres, L.F. Garfias-Mesías, D.R. Paul, Thermal degradation of commercially available organoclays studied by TGA–FTIR, Thermochim. Acta. 457 (2007) 92–102.
[36] S.A. Hashemifard, A.F. Ismail, T. Matsuura, Effects of montmorillonite nano-clay fillers on PEI mixed matrix membrane for CO_2 removal, Chem. Eng. J. 170 (2011) 316–325.
[37] T.S. Chung, X. Hu, Effect of air-gap distance on the morphology and thermal properties of polyethersulfone hollow fibers, J. Appl. Polym. Sci. 66 (1997) 1067–1077.
[38] P. Sukitpaneenit, T.S. Chung, Molecular elucidation of morphology and mechanical properties of PVDF hollow fiber membranes from aspects of phase inversion, crystallization and rheology, J. Membr. Sci. 340 (2009) 192–205.
[39] P. Sukitpaneenit, T.S. Chung, PVDF/nanosilica dual-layer hollow fibers with enhanced selectivity and flux as novel membranes for ethanol recovery, Ind. Eng. Chem. Res. 51 (2011) 978 – 993.
[40] M. Rezaei, A.F. Ismail, S.A. Hashemifard, T. Matsuura, Preparation and characterization of PVDF-montmorillonite mixed matrix hollow fiber membrane for gas–liquid contacting process, Chem. Eng. Res. Des. (2014), http://dx.doi.org/10.1016/j.cherd.2014.02.019.
[41] B.J.M. Oades, W.N. Townsend, The use of piperidine as an aid to clay-mineral identification, Clay Miner.Bull. 29 (1962) 177-182
[42] F. Liu, N.A. Hashim, Y. Liu, M.R.M. Abed, K. Li, Progress in the production and modification of PVDF membranes, J. Membr. Sci. 375 (2011) 1–27.
[43] Y. Shen, A.C. Lua, Preparation and characterization of mixed matrix membranes based on PVDF and three inorganic fillers (fumed nonporous silica, zeolite 4A and mesoporous MCM-41) for gas separation, Chem. Eng. J. 192 (2012) 201–210.
[44] Salavagione HJ, Martinez G, Ellis G. Graphene-based polymer nanocomposites. In: Mikhailov S, editor. Physics and applications of graphene experiments, Vol. 1. Rijeka (Croatia): Intech; 2010. p. 169–92
[45] M. Rezaei, A.F. Ismail, S.A. Hashemifard, G. Bakeri, T. Matsuura, Experimental study on the performance and long-term stability of PVDF/montmorillonite hollow fiber mixed matrix membranes for CO_2 separation process, Int. J. Greenh. Gas Control. 26 (2014) 147–157.
[46] R.N. Wenzel, Resistance of solid surfaces to wetting by water, Ind. Eng. Chem. 28 (1936) 988–994.
[47] A.B.D. Cassie, S. Baxter, Wettability of porous surfaces, Trans. Faraday Soc. 40 (1944) 546–551.

[48] T.T. Chau, W.J. Bruckard, P.T.L. Koh, A.V Nguyen, A review of factors that affect contact angle and implications for flotation practice, Adv. Colloid Interface Sci. 150 (2009) 106–15.
[49] S. Adnan, M. Hoang, H. Wang, Z. Xie, Commercial PTFE membranes for membrane distillation application: Effect of microstructure and support material, Desalination. 284 (2012) 297–308.
[50] H. Susanto, Towards practical implementations of membrane distillation, Chem. Eng. Process. Process Intensif. 50 (2011) 139–150.